Interplay between internal stresses and matrix stiffness influences hydrothermal ageing behaviour of zirconia-toughened-alumina

C. Wei, G. Montagnac, B. Reynard, Nathalie Le Roux, Laurent Gremillard

Interplay between internal stresses and matrix stiffness influences hydrothermal ageing behaviour of zirconia-toughened-alumina.

Published in: Acta Materialia 185 pp. 55-65, 2020
https://doi.org/10.1016/j.jeurceramsoc.2019.06.013

C. Wei[a,b], G. Montagnac[c], B. Reynard[c], N. Le Roux[b,d], L. Gremillard[b,*]

[a] School of Mechanics, Civil Engineering and Architecture, Northwestern Polytechnical University, 127 West Youyi Road, Beilin District, Xi'an Shaanxi, 710072, P. R. China
[b] Univ Lyon, INSA-Lyon, CNRS, MATEIS, UMR 5510, 20 avenue Albert Einstein, F-69621 Villeurbanne cedex, France
[c] Univ Lyon, ENS-Lyon, CNRS, LGL-TPE, UMR 5276, 46 allée d'Italie, F-69364 Lyon cedex 07, France
[d] Mécanium, 66 boulevard Niels BOHR CS 52132, F-69603 Villeurbanne cedex, France

* Corresponding Author: L. Gremillard (laurent.gremillard@insa-lyon.fr; Phone +33(0)472438152)
C. Wei : chong.wei@nwpu.edu.cn
G. Montagnac: gilles.montagnac@ens-lyon.fr
B. Reynard : bruno.reynard@ens-lyon.fr
N. Le Roux: payraudeaunathalie@yahoo.fr

Declarations of interest: none

Keywords: Zirconia-toughened alumina; Residual stresses; Durability; Raman spectroscopy

Abstract

Zirconia based bio-ceramics such as ZTA (Zirconia-toughened alumina) composite are often used in orthopaedic and dental implants. The hydrothermal ageing behaviour of zirconia in humid environments is an important factor affecting the lifetime of these biomaterials. It is a tetragonal-to-monoclinic phase transformation that has been shown to be both temperature- and stress-dependant. Here, ZTA composites with zirconia inclusion particles of different sizes were prepared. The influence of zirconia inclusions on internal stresses and thus on ageing behaviour was studied by Raman micro-spectroscopy and X-ray diffraction. The results show that the ageing kinetics result from a balance between stiffer matrix and increased tensile stress in the zirconia inclusion as the local alumina fraction increase. As a result, the maximum monoclinic fraction formed after1200 h ageing at 134°C decreases with increasing alumina content, showing the predominance of the stabilization of tetragonal particles by a stiff matrix over their de-stabilization by tensile stress.

1. Introduction

Zirconia-Toughened-Alumina (ZTA) composites are increasingly used for the fabrication of medical implants, mainly in the orthopaedic and dental field. Hydrothermal ageing (also called LTD for Low Temperature Degradation), one of their most relevant degradation mechanism in the human body, has been the topic of numerous studies in recent years. It consists in a thermally activated tetragonal-to-monoclinic (t-m) phase transformation in the presence of water, potentially leading to roughness increase and microcracking. The ageing process is affected by many factors, such as the proportion of zirconia, the nature and content of the stabilizing oxide in the zirconia phase, the density, surface finish, grain size, cubic/monoclinic zirconia ratio, stress, etc. [1].

The hydrothermal ageing behaviour of zirconia monoliths has been extensively studied, although not yet fully understood. Many studies hinted that residual or applied tensile stresses accelerate hydrothermal ageing. Indeed, since stress induced tetragonal to monoclinic martensitic transformation leads to ~5% volume increase [2], such transformation should be favoured in the presence of tensile stress, which is consistent with previous works (see [3–6] for example). Acceleration of ageing in ZTA with respect to zirconia is expected because zirconia particles are systematically under tensile stress due to the difference of thermal expansion coefficient between alumina and zirconia, and tensile stresses accelerate ageing. However the opposite is observed, and ageing can even be completely suppressed in ZTA materials with low zirconia content. The threshold below which no ageing occurs depends on several factors, such as the stabilizer nature and content in the zirconia phase or the agglomeration state of the zirconia grains in the composite. For instance, threshold values are 7 vol.% when agglomerates are present [7] or 16 vol.% when there are no zirconia agglomerates [8]. Thus the role of stresses in the hydrothermal ageing process of zirconia-toughened alumina is not yet fully understood. Since the pioneering work by Lange [9] matrix stiffness is known to be an important factor controlling the t-m transformation in zirconia. However to our knowledge this factor has not been evaluated yet in the framework of hydrothermal ageing.

Most researches on zirconia ageing have been conducted using X-ray diffraction (XRD) to characterize the tetragonal-to-monoclinic transformation. However, XRD lacks in spatial resolution. Micro-Raman spectroscopy has micrometric spatial resolution, and Raman spectra contain information on the symmetry and stress state of the examined material. Raman microspectroscopy is thus a powerful technique to study the spatial distribution of both zirconia phases and residual stresses in zirconia ceramics. Stress state of tetragonal zirconia is often determined using shifts in the position of the Raman band located at 146 cm^{-1} in the tetragonal phase [10]. Micro-Raman gives information on local residual stresses, for example residual stresses within a deformation band in a ceria-stabilized tetragonal zirconia and alumina [11], or inside a multilayered composites consisting of Al_2O_3/3Y-TZP (3 mol% Y_2O_3-stabilized ZrO_2) layers [12].

In the present study, we analyse the stress state of the zirconia inclusion particles in zirconia toughened alumina (ZTA) composites and their ageing behaviour, in order to quantify the effect of stresses on the hydrothermal ageing of zirconia inclusions in ZTA. In order to apply different levels of stresses on zirconia, composites with different amounts of zirconia (thus different Young modulus of the matrix) and with different particle sizes were synthesized. Ageing is then examined globally using XRD, and locally using micro-Raman spectroscopy.

2. Materials and methods

2.1. Material preparation

The ZTA samples were prepared from 3 mol% Y_2O_3 co-precipitated zirconia powder (TZ-3Y, Tosoh, Japan) and high purity alumina powder (AKP50, Sumitomo, Japan), with mixing ratios of either 10 vol.% or 25 vol.% zirconia (respectively referred to as ZTA10- and ZTA25-materials). The powders were dispersed in water by ball-milling with zirconia balls, using Darvan 821A (Vanderbilt Minerals LLC) as a dispersing agent. In order to prepare several materials containing zirconia with different aggregates sizes, different mixing schedules were used:

- Co-milling zirconia and alumina powders during 7 days (referred to as "ZTA25-7d-" materials), or
- Co-milling zirconia and alumina powders for 1 day (referred to as "ZTA25-1d-" materials), or
- Milling alumina powder alone for one day, and then adding zirconia powder and milling again for 8 minutes (referred to as "ZTA10-1d8m-" and ZTA25-1d8m-".

The mixed slurries were then cast in porous plaster moulds and dried until composite green bodies were obtained. Then the cast green bodies were debinded and sintered in a programmable electrical furnace (first dwell of 5h at 550°C (1°C/min heating ramp), then heating at 5°C/min to a second dwell at1430°C for 3 h, and finally cooling down to room temperature at 5°C/min). The samples were then wet-polished with 1200 and 2400 grit paper and mirror-polished with diamond pastes (down to 1µm) (suffix "P"). Note that the polishing procedure was conducted so that some stresses remain after polishing while all samples present the same, small roughness. Consequently, some of the polished samples were annealed (suffix "A") to remove as much as possible the remaining machining and polishing residual stresses (1250°C for 0.5h at 5°C/min [13]). The samples studied here are summarized in Table 1.

Table 1 : ***Samples prepared for the study of internal stress. The symbols indicated in the table will be used throughout this article.***

Zirconia amount	Milling procedure		
	7d	1d	1d8min
25vol.%	ZTA25-7d-A ■	ZTA25-1d-A ●	ZTA25-1d8m-A ▲
	ZTA25-7d-P □	ZTA25-1d-P ○	ZTA25-1d8m-P △
10vol.%			ZTA10-1d8m-A ◆
			ZTA10-1d8m-P ◇

2.2. X-ray diffraction

The amount of monoclinic phase was measured by X-ray diffraction using a D8 advance Diffractometer (Bruker, Germany) equipped with a LynxEye linear detector, with Kα radiations, in Bragg-Brentano configuration. XRD patterns were recorded in the 27-33° (2θ) range with a scan speed of 3 °·min^{-1} and a step size of 0.05°. The monoclinic ZrO_2 phase content (V_m) was expressed after Toraya's equation [14]:

$$V_m = \frac{1.311X_m}{1 + 0.311X_m} \quad (1)$$

In which the value of X_m was calculated using Garvie and Nicholson method [15]:

$$X_m = \frac{I_m^{-111} + I_m^{111}}{I_m^{-111} + I_m^{111} + I_t^{101}} \quad (2)$$

Where I_p^{hkl} is the area of the diffraction peak related to the (hkl) plane of phase p (m for monoclinic and t for tetragonal).

The crystallographic texture of the tetragonal phase is often characterized by the $I_t^{(002)}/I_t^{(110)}$ ratio [16,17]. In ZTA measuring directly this ratio is impossible because the (110) peak of tetragonal phase and (104) peak of corundum are superimposed. Thus Rietveld refinement was used to more accurately measure the intensities of these peaks, using the Topas 4.0 software. The refinement took into account tetragonal and cubic zirconia phases as well as α-alumina. The texture of the tetragonal phase was described by the March-Dollase model implemented in Topas. The intensities of the (110) and (002) tetragonal peaks were retrieved from the diffraction diagram of the tetragonal phase calculated by Topas. The refinement were conducted on XRD diagrams recorded in the 20-70° (2θ) range with a scan speed of 1.2 °·min^{-1} and a step size of 0.02°.

2.3. Raman spectroscopy

The amount of tetragonal to monoclinic phase transformation was measured by Raman spectroscopy on a Horiba Jobin-Yvon LabRAM HREvolution microspectrometer with a maximum spatial resolution of 0.5 µm. The Raman spectra were recorded from 90 to 600 cm^{-1}, using a laser with 532 nm wavelength. The monoclinic phase content (Vm) was calculated according to the formula proposed by Muñoz-Tabares and Anglada [18]:

$$V_m = \frac{I_m^{179} + I_m^{190}}{(I_m^{179} + I_m^{190}) + 0.32(I_t^{146} + I_t^{256})} \quad (3)$$

Where I_p^{wn} is the area of the peak related to the Raman shift of the characteristic bands (at wave number *wn*) of phase p (m for monoclinic and t for tetragonal). Typical Raman spectra of the powders used in this study are shown on Figure 1.

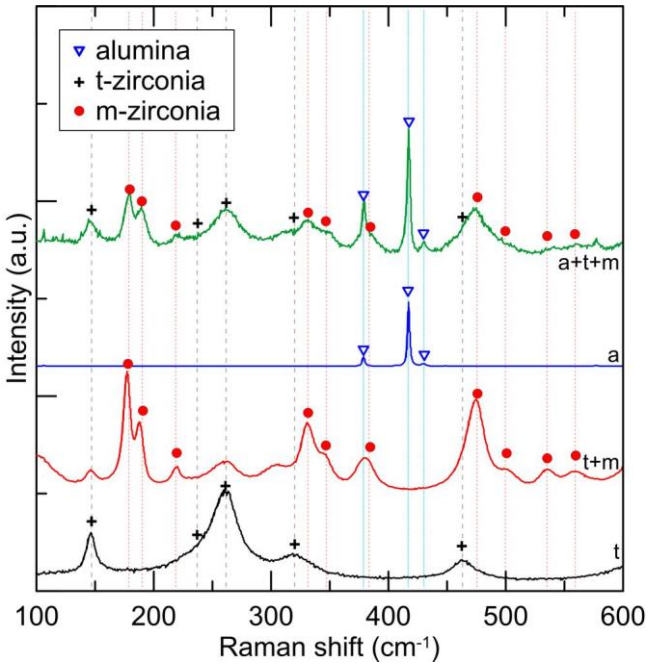

Figure 1 : Typical Raman spectra of tetragonal zirconia (t, obtained on TZ-3Y powder calcined at 1200°C)), a mixed tetragonal and monoclinic zirconia (t+m, obtained on the as-received TZ-3Y powder), alumina (obtained on the AKP50 powder), and a mixture of tetragonal + monoclinic + alumina phases (a+t+m, obtained on a ZTA25-1d-8m-P composite after 1200h ageing) from 90 to 600 cm^{-1}.

The microscopic stress distribution was measured by collecting Raman spectra over linear or two-dimensional arrays on the samples surface. The automatically collected arrays of spectra in relatively large two-dimensional maps were typically 5 µm-spaced and the laser spot size was about 1 µm. In previous reports [10,19,20], it was found that the stress in the crystal phase has an approximately linear relationship with its associated spectral shift (Δν), as:

$$\Delta\nu = 3\Pi_\upsilon \sigma_p \qquad (4)$$

Where σ_p is the average normal stress of the phase p, Π_ν is uniaxial piezo-spectroscopic coefficient corresponding to the characteristic band, Δν is the spectral offset. Since Π_u of each characteristic band is constant, a quantitative analysis of stresses can be conducted by measuring the spectral offset Δν.

The spectral offset of the 146 cm^{-1} band was used for stress assessment in tetragonal zirconia, with a value of Π_υ = -0.6 cm^{-1}/GPa [10], the position of the same band measured on TZ-3Y powder being taken as the corresponding stress-free position.

The local alumina volume fraction (V_a) is determined on the same spot from the proportion of relevant peaks areas as shown in the following equation:

$$V_a = \frac{\mathrm{k}\times I_a^{417}}{\mathrm{k}\times I_a^{417}+(I_m^{179}+I_m^{190})+0.32(I_t^{146}+I_t^{256})} \qquad (5)$$

where I_p^{shift} is the area of the peak related to the Raman shift of the characteristic bands of phase p (m for monoclinic, t for tetragonal and a for alumina phase) and k is a constant that will be evaluated in the present article.

Since several thousands Raman spectra were obtained, an automated analysis procedure was devised, that used the fitting ability of Topas 4.0 Rietveld analysis software (Bruker, Germany). Basically, Raman spectra were transformed to a file format usable by Topas by a simple Matlab routine. Topas was then used in a batch mode to extract the position (centre, ν_0), intensity (I_0), width (h) and shape factor (η) of all the peaks present on the spectra (all peaks being considered as pseudo-Voigt functions, eq. 6) and related to either alumina, monoclinic zirconia or tetragonal zirconia (for each phase, a complete list of the characteristic peaks with approximate parameters was provided to Topas as initial conditions for the fit). Finally, for each spectrum the procedure returned a restricted list of the parameters necessary for the use of equations 3, 4 and 5 (*i.e.* $I_m^{179}, I_m^{190}, I_t^{146}, I_t^{256}, I_a^{417}, \nu_0^{146}$). However this procedure is not perfect, and sometimes leads to slight overestimation of the background,

resulting in artificially negative values for V_m for small monoclinic phase fraction (< 3 vol. %).

$$I=I_0\left[(1-\eta)\frac{\sqrt{4ln2}}{h\sqrt{\pi}}\exp\left(\frac{-4ln2.(\upsilon-\upsilon_0)^2}{h^2}\right)+\eta\frac{2h}{\pi(1+4(\upsilon-\upsilon_0)^2)}\right] \quad (6)$$

2.4. Assessment of ageing kinetics

Ageing kinetics were evaluated by performing accelerated ageing tests on all samples in water steam at 134 ◦C, under 2 bars pressure. The hydrothermal ageing kinetics are rationalized by fitting the t-m transformation curves with the Mehl–Avrami–Johnson laws [21]:

$$f=\frac{V_m-V_0}{V_{Max}-V_0}=1-\exp(-(bt)^n) \quad (7)$$

where V_m is the monoclinic phase content, V_0 and V_{Max} are respectively the initial and saturation levels of monoclinic phase content, b is a thermally activated kinetic parameter (whose activation energy could not be measured here).

2.5. Microstructural observations

Microstructures were observed using scanning electron microscopy (SEM, ZEISS Supra55-VP, Germany) without conductive coating, in high vacuum at low accelerating voltage (2 kV). The average grain size of zirconia and alumina in the annealed samples was calculated from measurement of at least 500 grains selected randomly. The average size of zirconia agglomerates was obtained from about 200 agglomerates selected randomly.

3. Results

3.1. Microstructure

Figure 2 shows micrographs of all ZTA specimens. Quantification of their microstructures is reported in Table 2. The average grain sizes of zirconia and alumina in ZTA25-7d sample are smallest. In both 1d8m samples, the dispersion of zirconia agglomerates was not complete, and big zirconia agglomerates remain together with well dispersed small zirconia grains. Interestingly, the size of zirconia grains in the agglomerates is larger than the size of dispersed grains.

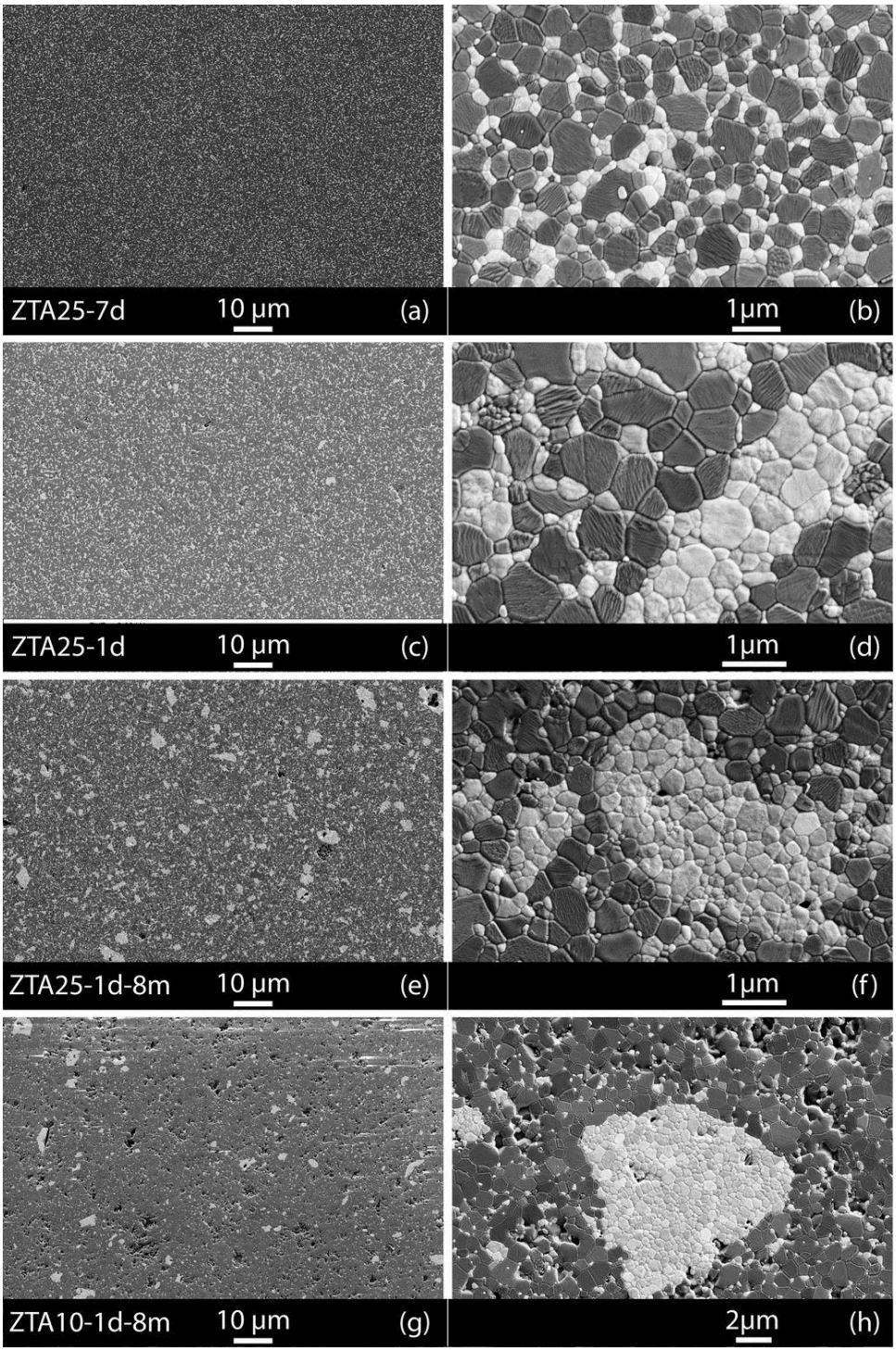

Figure 2 : SEM images of all ZTA specimens.

Table 2 : microstructural features of ZTA materials (NA: not applicable)

Material	ZTA25-7d	ZTA25-1d	ZTA25-1d8m	ZTA10-1d8m
Alumina grain size (µm)	0.58±0.21	0.67±0.26	0.66±0.25	0.78±0.32
Size of isolated zirconia grains (µm)	0.22±0.09	0.29±0.15	0.30±0.15	0.32±0.16
Size of zirconia grains in agglomerates (µm)	NA	0.40±0.15	0.43±0.17	0.44±0.17
Size of zirconia agglomerates (µm)	NA	2.1±1.1	4.6±3.0	3.5±2.7
Fraction of total zirconia in agglomerates (estimation)	NA	0.01	0.15	0.35

3.2. Quantitative analysis of Al_2O_3 phase in ZTA by Raman Spectroscopy

In order to quantify the alumina content, the constant *k* in equation (5) has to be determined. Since the zirconia distribution in ZTA25-7d samples is very homogeneous, and the volume fraction of the alumina phase is known (75%), this sample was used to determine *k*. A value of 29.3 was obtained from 722 Raman spectra of ZTA25-7d samples.

3.3. Analysis of texture before ageing

Figure 3(a) shows an example of decomposition of XRD diagram into the diagrams of the constituent materials (alumina, tetragonal and cubic phases), and taking into account a possible texture (possible inversion of the $I_t^{(002)}/I_t^{(110)}$ ratio as compared to the theoretical ratio). It shows that even in the case of the largest measured texture (ZTA25-7d-A, shown here) the intensities are not inverted, thus the texture is not very large. As shown in Figure 3(b), the ratios measured here are between 0.65 and 0.88, whereas the same ratio measured in a nanometric, non-textured 3Y-TZP powder is 0.68 and the theoretical value is 0.64.

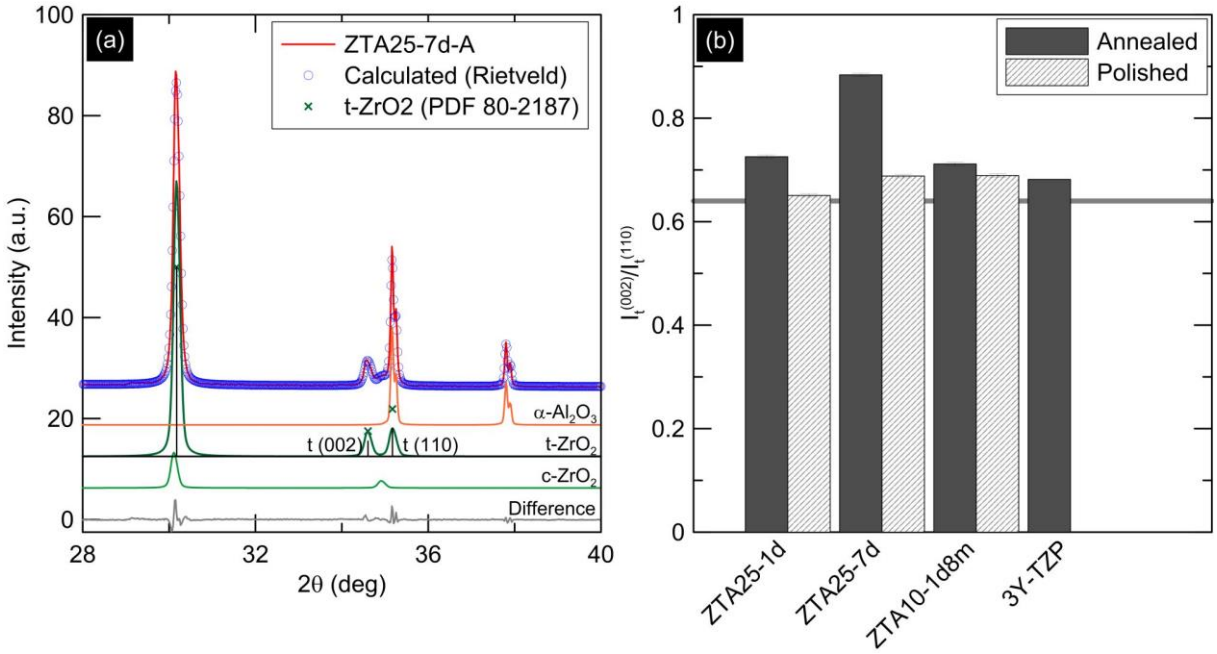

Figure 3 : (a) Rietveld refinement of XRD of ZTA25-7d-A, showing a slight texture (deviation from the theoretical intensity ratio between the (002) and (110) tetragonal peaks); (b) It(002)/It(110) ratio for all materials.

3.4. Analysis of internal stress before ageing

XRD results show that the surface of all samples before ageing test is mainly composed of alumina phase and zirconia tetragonal phase.

Stress analysis in inclusion-free composites

With the uniform distribution of zirconia in ZTA25-7d and ZTA25-1d samples, the Raman spectra of these samples were collected (ZTA25-7d-A, 53 points; ZTA25-7d-P, 620 points; ZTA25-1d-A, 339 points; ZTA25-1d-P, 289 points). The resulting estimates of stress are shown in Table 3 and Figure 4. It was also found that the zirconia particles mixed in the alumina are mainly subjected to tensile stress, and that polishing process both lowers the average internal tensile stress and increases the width of the distribution of the internal stress. In addition, small amounts of monoclinic zirconia (0 to 20%) were found on some few isolated grains of ZTA25-7d-P and ZTA25-1d-P.

Table 3 : Average spectral shift and stress in ZTA25-7d and ZTA25-1d samples

sample name	Nº of measuring points	spectral shift Δν(cm^{-1}) ± standard deviation	Stress (MPa) ± standard deviation
ZTA25-7d-A	53	-1.5±0.092	833±51
ZTA25-7d-P	620	-1.17±0.274	650±152
ZTA25-1d-A	339	-1.34±0.085	744±47
ZTA25-1d-P	289	-1.21±0.165	672±92

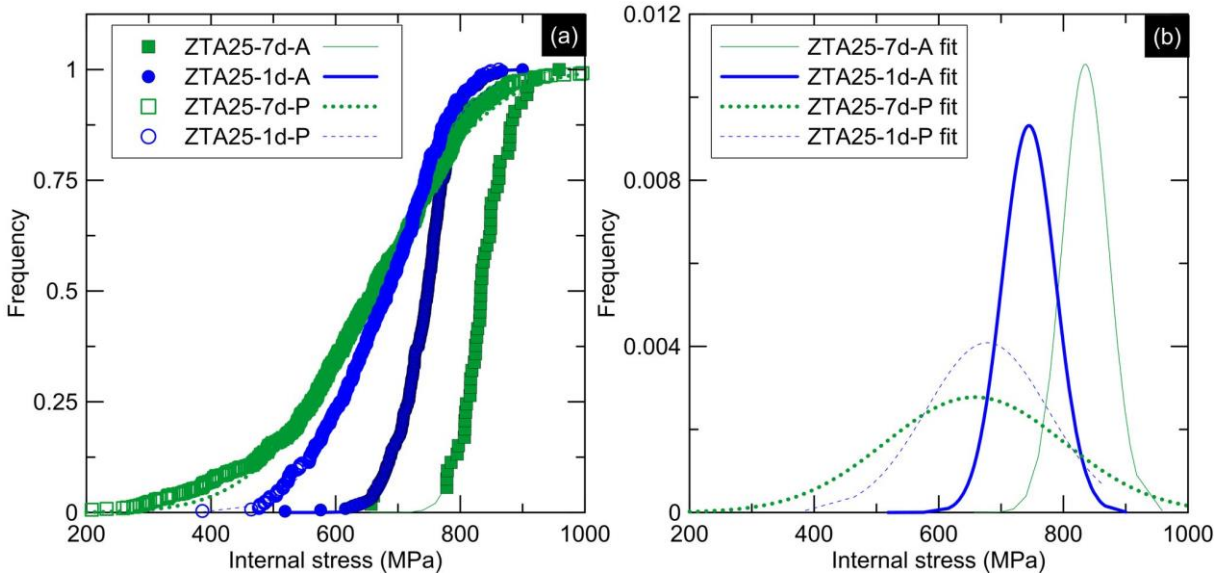

Figure 4: distribution of internal stresses in the t-phase at each point on the surface of the samples (ZTA25-7d and ZTA25-1d)

*Stress analysis of large zirconia inclusions (>2*2µm)*

In the four materials ZTA10-1d8m-A, ZTA10-1d8m-P, ZTA25-1d8m-A and ZTA25-1d8m-P, zirconia inclusions were large enough to collect Raman maps, allowing the quantification of monoclinic fraction, alumina fraction and residual stress in the tetragonal phase (Figure 5). In all these 4 materials, the centres of the large inclusions show the presence of monoclinic phase, especially in polished samples, and lowest tensile stresses. The polishing process seems to favour the presence of monoclinic phase. Moreover, a small amount of monoclinic zirconia appeared in ZTA10-1d8m-A samples (but not in ZTA25-1d8m-A samples).
Zirconia has a smaller tensile stress in ZTA25-1d8m-A than in ZTA10-1d8m-A sample. This hints to an effect of the composition on the presence of monoclinic phase: higher alumina fraction in the matrix leads to greater internal stresses in the zirconia particles. Thus, in order to better study the effect of alumina volume fraction on the residual stress in tetragonal zirconia particles, we chose to analyse the Raman spectra of the two annealed samples (ZTA25-1d8m-A and ZTA10-1d8m-A), excluding spectra containing monoclinic zirconia from the comparison, since the t-m transformation can dramatically change the stress state around the transformed grains. The results show that the tensile stress in zirconia grains increases almost linearly with local alumina fraction (Figure 6).

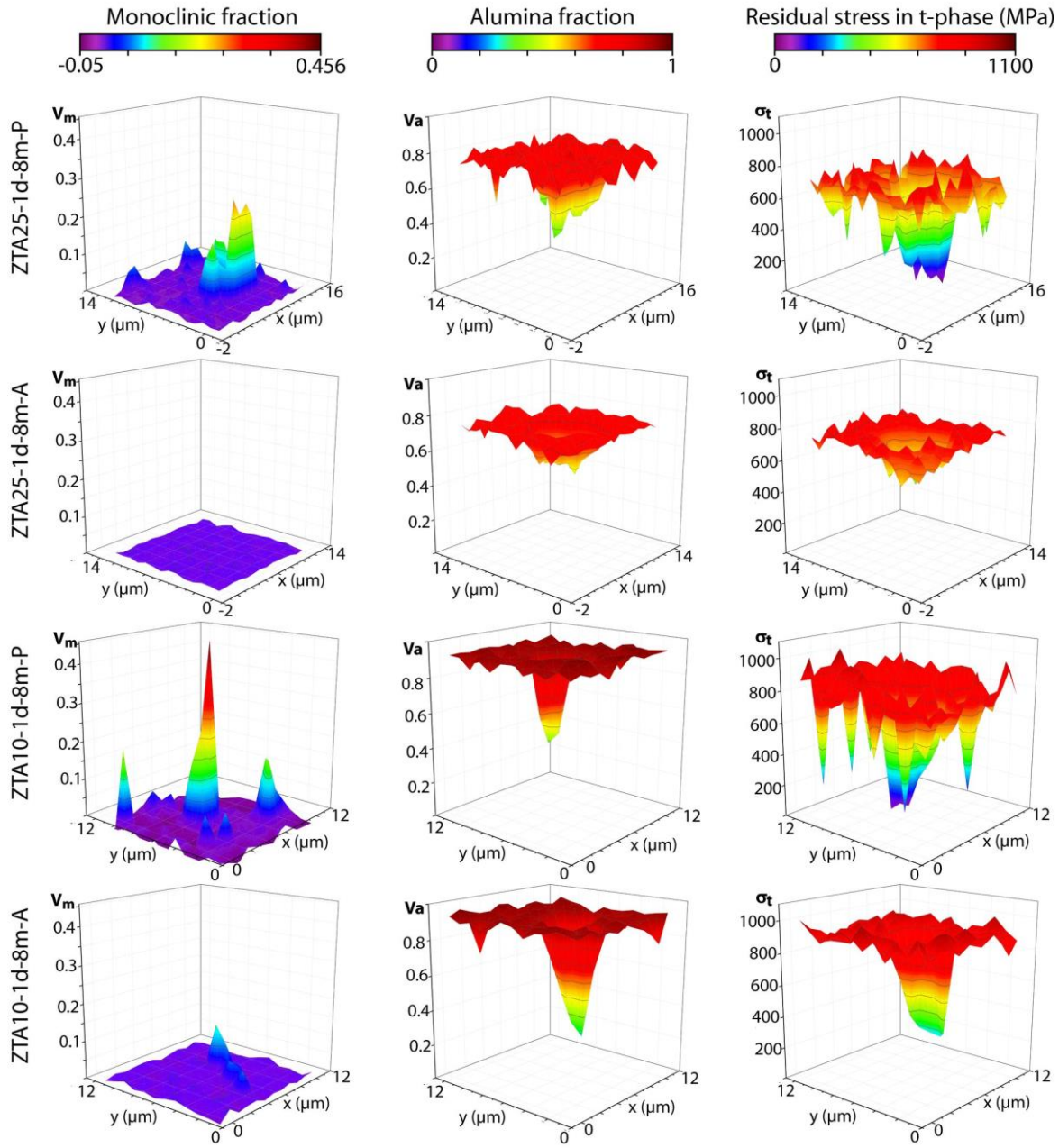

Figure 5 : examples of monoclinic fraction (Vm), alumina volume fraction (Va) and residual stress in tetragonal phase distribution on the surface of large zirconia inclusions and their surroundings in ZTA25-1d-8m and ZTA10-1d-8m samples before ageing.

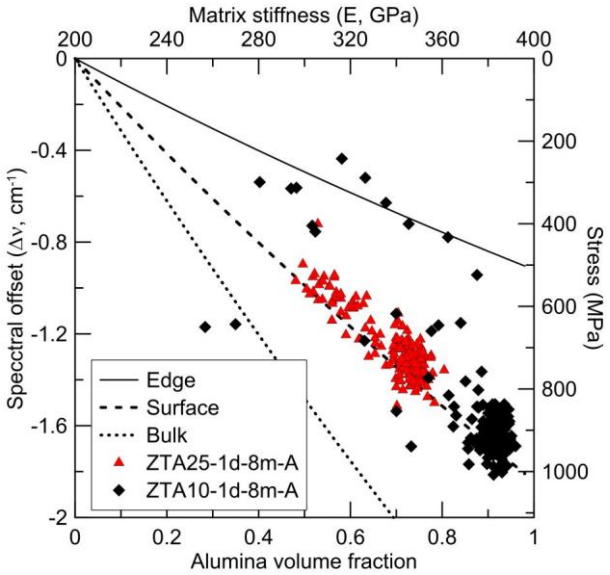

Figure 6 : Spectral shift of the 146 cm-1 t-zirconia band (proportional to residual stress) versus local alumina volume fraction (or local stiffness) in ZTA25-1d8m-A and ZTA10-1d8m-A samples (only annealed samples are included since the others present monoclinic phase that would bias the data). The three dashed lines are the residual stresses expected to be measured using eq. 4, depending on their location: on an edge, in the surface or in the bulk (equation (9 and 10) in the discussion).

3.5. Ageing process

After ageing at 134 °C for 1000 hours, ZTA25-7d-A and ZTA25-1d-A samples do not show any trace of monoclinic phase according to XRD data. The ageing kinetics of other samples are shown in Figure 7. Generally all ageing kinetics are slow compared to conventional, monolithic 3Y-TZP zirconia. The maximum monoclinic content after 1000 h ageing at 134 °C is 15% (Figure 7). Table 4 reports the parameters of the Mehl-Avrami-Johnson equation used to described ageing kinetics (eq. 7). Values of n lower than 1 point to ageing kinetics dominated by nucleation of the monoclinic phase [22] (which is coherent with the structure of the material, in which growth of the monoclinic nuclei is hardly possible). No correlation could be found between n, b and the initial average internal stress measured from the average spectral shift of the 146 cm^{-1} band of t-ZrO_2. However, strong correlations between V_{Max} and the initial stress and between V_0 and the initial stress exist, as it is illustrated on Figure 8 that reports V_{Max}-V_0 *vs* initial internal stress. This figure shows a threshold between 700 and 750 MPa above which ageing does not occur anymore, while below the threshold the saturation monoclinic fraction decreases linearly with increasing internal stress.

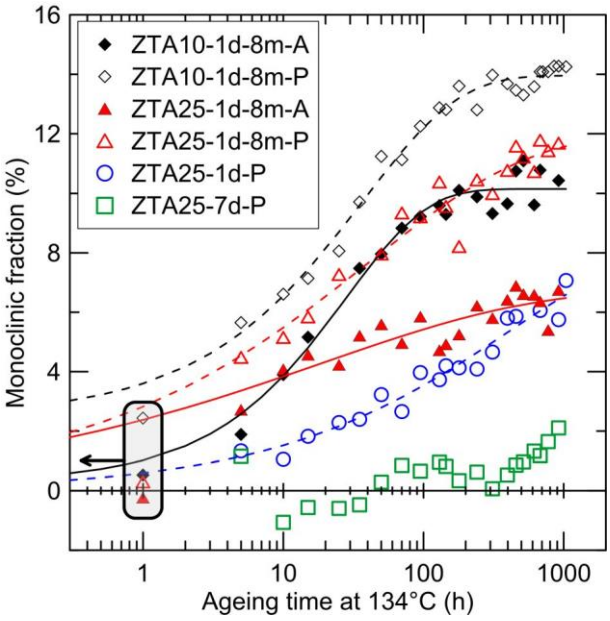

Figure 7 : XRD monoclinic fraction measured versus ageing time (the initial state, time 0, is shown at time 1h (rectangle and left-pointing arrow) because of the impossibility to represent time 0 in logarithmic scale)

Table 4 : Parameters of the Mehl–Avrami–Johnson laws for the materials susceptible to ageing (n, b, V_0, V_{Max}). Ageing of ZTA25-7d was too slow to determine its parameters.

Material	ZTA25-1d-P	ZTA25-1d-8m-A	ZTA25-1d-8m-P	ZTA10-1d-8m-A	ZTA10-1d-8m-P
n	0.44	0.29	0.38	0.77	0.63
B	0.0024	0.053	0.025	0.035	0.027
V_0 (%)	0	0	0.24	0.3	2.5
V_{Max} (%)	8.5	6.8	12.0	10.1	14.0
Initial internal stress (MPa)	673.36	702.45	579.95	623.56	547.17

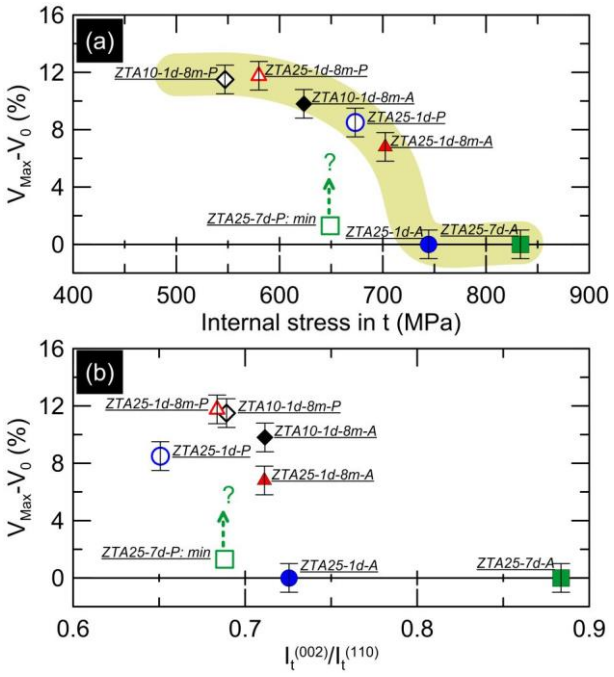

Figure 8 : (a) Maximum possible t-m transformation by ageing at 134°C versus average initial internal stress (the point for ZTA25-7d-P is the minimum possible value (e.g. maximum measured monoclinic content), since V_{Max} could not be measured for this material). The error bars indicate an estimation of the uncertainty of 1% (absolute uncertainty); (b) Maximum possible t-m transformation by ageing at 134°C versus texture parameter.

3.6. Phase analysis of large zirconia inclusions after ageing

The monoclinic fraction measured at several points of ZTA10 (Figure 9a) or ZTA25 (Figure 9b) samples varies with the alumina volume fraction measured on the same points. Since the maximum t-m transformation extension varies linearly with the average initial internal stress in the composite (Figure 8), and the average internal stress in ZTA10 samples and ZTA25 samples are different, the two groups of materials are discussed separately.

In ZTA10 samples, the maximum monoclinic fraction exhibits a non-linear decrease with increasing alumina content: large zirconia agglomerates, corresponding to alumina fraction lower than 60 vol.%, are fully transformed to monoclinic after 1000h ageing; on the contrary, when zirconia is fully dispersed inside the alumina matrix (alumina fraction at its maximum, nominal 90%), it remains almost completely tetragonal and does not suffer from ageing.

In ZTA25 samples, the maximum monoclinic fraction decreases more progressively with increasing alumina content (although one should point out a bias in the statistics, as fewer big zirconia inclusions were found in ZTA25 than in ZTA10). In both groups of materials, the same trend is seen whatever the treatment (polished or annealed) and whatever the overall microstructure (1d-8m or 1d). Note that 7d materials are not reported in Figure 9 since they are completely homogenous and do not age, they would overlap with the large group of points at V_m~0 and V_a=0.9 (for ZTA10) or 0.75 (for ZTA25). XRD results are consistent with these trends.

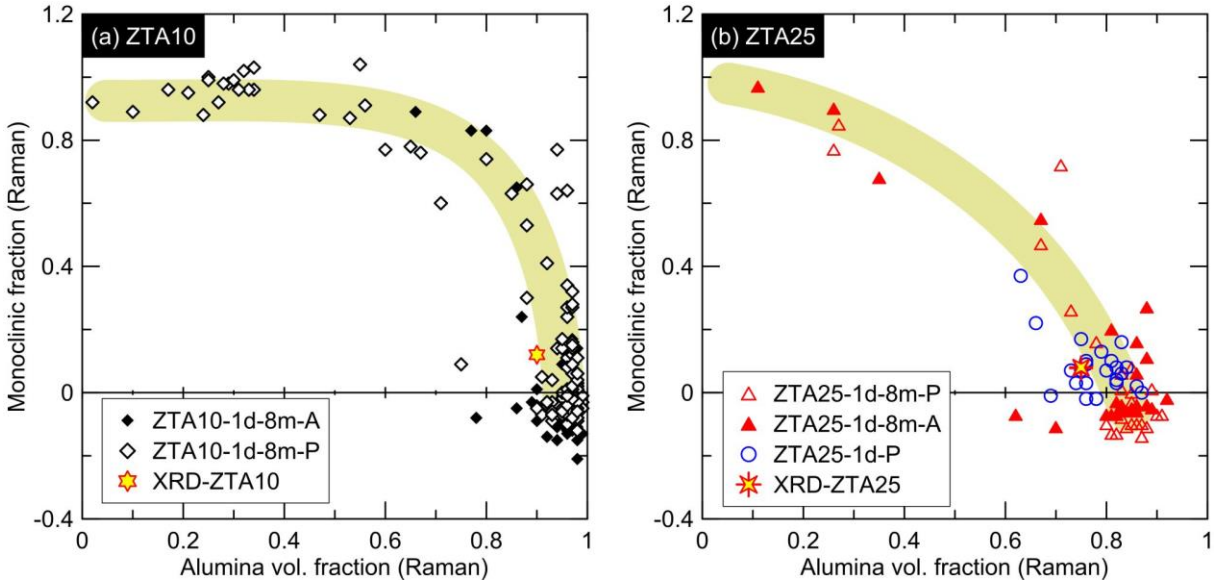

Figure 9 : Monoclinic zirconia fraction versus alumina volume fraction (measured by Raman spectroscopy, using equations 3 and 5) after ageing 1200h at 134°C. (a): ZTA10-1d8m; (b): ZTA25 samples. The X-Ray diffraction points are average values on all ZTA10 materials (a) or all ZTA25 materials (b) after the same ageing treatment. The thick, yellow lines are only guides for the eyes.

4. Discussions

4.1. Effect of texture

In this work all samples were characterized either after polishing or after polishing followed by annealing. In zirconia, rough polishing treatments are known to induce plastic deformation in a thin surface layer. Annealing these polished materials can induce a recrystallization into very small crystallites [23,24], and sometimes the apparition of a texture seen by XRD as modification of the $I_t^{(002)}/I_t^{(110)}$ ratio [16,17] (theoretically, from the structure factors of these two peaks this ratio is around 0.6, but it can vary up to 2.5 in the case of an important texture). This texture is associated to ferroelastic domain switching under the effect of large compressive stresses. Moreover, this surface microstructure is thought to slow down ageing kinetics [16,17,23,24], which is attributed either to the small grains [16,24], to the large, compressive residual stresses [17] that are also the cause of ferroelastic domain switching, or to the texture itself [16]. In any case, the direct, physical link between texture and hydrothermal ageing is difficult to establish with complete certainty.
Here, $I_t^{(002)}/I_t^{(110)}$ ratio between 0.65 and 0.88 were found, much lower than what was found in the articles cited above. Moreover, Figure 8 shows a much nicer correlation between the t-m transformation extension after ageing and the initial residual stress (a) than between the transformation extension and the texture (b). Without ruling out a possible effect of the texture (because of limited number of materials), this shows that the initial stresses have more impact than texture on the ageing kinetics, at least in the ZTA materials studied here.

4.2. Effect of alumina content

The influence on internal stress before ageing

Our results show that the internal stress of zirconia in tetragonal zirconia and alumina two-phase composite increases with increasing alumina content, which is consistent with previous studies [12,25].The residual hydrostatic stress of isolated zirconia particles in tetragonal zirconia and alumina two-phase composite after cooling down from sintering temperature can be written as [11,26,27]:

$$\sigma_t^p = -\frac{V_a}{1-V_a} \times \frac{3K_a(\alpha_t-\alpha_a)\Delta T V_a(1+n_a)}{(1-V_a)(1+n_a)+V_a(1+n_a\frac{K_a}{K_t})}, \qquad n_a = \frac{2(1-2\nu_a)}{(1+\nu_a)} \qquad (8).$$

In equation (8),σ_t^p is the internal stress of zirconia particle in ZTA composites, caused by the thermal expansion mismatch between alumina and zirconia phases, K_t, K_a are the bulk modulus of zirconia and alumina phase (184 GPa and 247 GPa respectively [28]), α_t, α_a are the thermal expansion coefficients of the zirconia and alumina phase (typically $1 \cdot 10^{-5}$ and $8 \cdot 10^{-6}$, respectively). ΔT is the difference between room temperature and the temperature on cooling down at which stress can no longer be relaxed (as a first approximation, we choose ΔT=-1200K), ν_t, ν_a are the Poisson ratio of zirconia and alumina (0.31 and 0.23, respectively, from [28] and Lamé's relation), and V_t, V_a are the volume fraction of zirconia and alumina phase in the composites, and their sum is 1. Equation (8) is valid only when zirconia particle are dispersed in a continuous alumina matrix, thus for large values of V_a.

The theoretical residual stresses (and the deduced Raman shift offset) calculated from equations (8) are reported in Figure 6 versus the alumina volume fraction (or local matrix stiffness), considering 3 cases: the bulk case (where equation (4) applies), the surface case where equation (4) should be replaced by equation (9) since $\sigma_{33} = 0$, and the 1D case (particle on the edge of a surface pore, $\sigma_{22} = \sigma_{33} = 0$) (any case between these limits is possible, given the small depth analysed by Raman spectroscopy).

$\Delta\nu_{2D} = 2\Pi_u\sigma_p$ (9)

$\Delta\nu_{1D} = \Pi_u\sigma_p$ (10)

The good agreement between experimental data and theoretical curves shown in Figure 6 shows that the residual stress in zirconia inclusions (or grains) depends more on local alumina content (local matrix stiffness over a few cubic micrometers, the size of the Raman probe used here) than on overall matrix stiffness, although this approach does not take into account the fact that the internal stress of the inclusions is related to the shape and size of the inclusions [29–32]. Data lie between the prediction for the 1D and bulk cases (and in few cases cose to the 1D case) but are close to the intermediate prediction for the surface case. Although this may reflect the fact that Raman measurements conducted here are mainly surface measurements, not too much credit should be given to this observation, since the calculated lines are very sensitive to small changes of ΔT, α_a and α_t.

The influence on ageing process

The maximum extension of t-m transformation after ageing decreases with the increase of alumina content, in consistency with former results [7]. Three main reasons account for these results: 1- when increasing the alumina content, the stiffness of the matrix around the tetragonal grains increases, the energy necessary to overcome the deformation resulting from the t-m transformation is higher, and the t-m transformation is more difficult; 2- when the alumina content increases, the matrix around zirconia grains gets stiffer and blocks the growth of micro-cracks caused by volume expansion during t-m zirconia phase transformation, reducing the diffusion channel of the water molecules between the zirconia grains; 3- with more alumina, the number of Al/Zr-VÖ bonds [33] (more stable than Y/Zr-VÖ) increases, which increases thermal activation energy, delaying ageing.

Increasing the alumina content also increases the residual tensile stresses in the zirconia grains (Eq. 8). Thus the decrease of t-m transformability with increasing alumina content is coherent with the decrease of transformability with increasing tensile stresses shown in Figure 7. This may seem contradictory with existing literature on zirconia, where residual tensile stresses favor the transformation (see [3–6] for example) – however the matrix stiffness is constant, unlike in ZTA. Here in ZTA, the largest tensile stresses are associated with the stiffest,

alumina-rich matrix, more difficult to deform, which might delay or prevent t-m transformation.

The work of Lange [9] already presents an analysis of the thermodynamic effects of matrix stiffness and residual stresses on the tetragonal-to-monoclinic phase transformation in zirconia. The difference of free energy (ΔG_{t-m}) between a tetragonal inclusion and the same inclusion after the t-m transformation is described by the following equation:

$$\Delta G_{t-m} = -\Delta G_c + \Delta U_{SE} + \Delta U_S \qquad (11)$$

Here ΔG_c is the chemical free energy (that depends on the temperature and on the composition, in particular in our case the amount of hydroxyl ions occupying the oxygen vacancies [34]), ΔU_{SE} is the elastic energy associated with the transformation, and ΔU_S is a surface energy term [9]. One can consider that matrix stiffness and residual stresses only impact ΔU_{SE}. Still following Lange's work, and considering the extreme case where the residual stresses maximally favor transformation, these effects can be accounted for by expressing ΔU_{SE} as:

$$\Delta U_{SE} = \frac{s}{6}\left(\frac{\Delta V}{V}\right)^2 + \sigma_{ij}^I \varepsilon_{ij}^r + \sigma_{ij}^r \varepsilon_{ij}^{tr} \qquad (12)$$

In this equation, σ_{ij}^I is the stress in the transformed inclusion, ε_{ij}^r and σ_{ij}^r are the residual strain and stress in the inclusion prior transformation, and ε_{ij}^{tr} is the transformation strain.

s is given by the equation:

$$s = \frac{2E_1E_2}{(1+\nu_1)E_2+2(1-2\nu_2)E_1} \qquad (13)$$

In equation (13), E_1, E_2, ν_1, ν_2 are respectively the Young's modulus and Poisson ration of the matrix (1) and transforming inclusion (2). These properties can be calculated using the equations by Pabst [28] (eq. (14a-b) and Lamé's relation (eq. 14(c)):

$$E_1 = 210.4 + 133.3V_a + 56.3V_a^2 \qquad (14a)$$

$$K_1 = 184.2 + 25V_a + 10.8V_a^2 \qquad (14b)$$

$$\nu_1 = \frac{1}{2} - \frac{E_1(V_a)}{6K_1(V_a)} \qquad (14c)$$

$$E_2 = E_t \qquad (14d)$$

$$\nu_2 = \nu_t \qquad (14e)$$

One should also consider that σ_{ij}^I depends on the alumina fraction, via the combination of equation (13), (14) and (15) derived from [9]:

$$\frac{s}{6}\left(\frac{\Delta V}{V}\right)^2 = \frac{1}{2}\sigma_{ij}^I \varepsilon_{ij}^{tr} \qquad (15)$$

As a result, the Figure 10 shows the variations of ΔU_{SE} with V_a when implementing the materials properties used in the first paragraph of the present section, E_a=400GPa and E_t=210 GPa (considering that all stresses and strains are hydrostatic and using 0.05 for $\Delta V/V$). ΔU_{SE} increases with the alumina fraction. This effect can be discomposed in two opposite ones. A first effect is an increase of ΔU_{SE} with stiffness (*e.g.* a less easy t-m transformation), seen by the term $\frac{s}{6}\left(\frac{\Delta V}{V}\right)^2$. The second effect results in a slight decrease of the part of ΔU_{SE} affected by residual stresses ($\sigma_{ij}^I \varepsilon_{ij}^r + \sigma_{ij}^r \varepsilon_{ij}^{tr}$) when increasing the residual tensile stress, in coherence with an easier transformation in the presence of tensile stresses. The later effect is clearly dominated by the effect of stiffness.

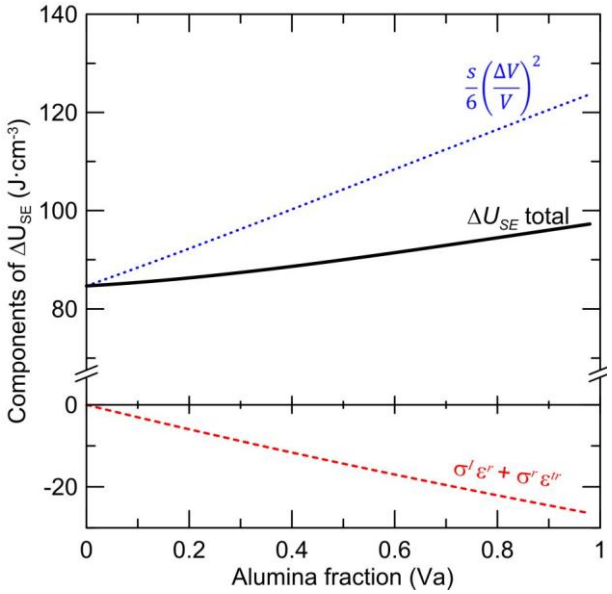

Figure 10 : evolution of ΔU_{SE} (bold, black line) with Va, showing the distinct effects of residual stresses (dashed, red line) and matrix stiffness (dotted, blue line)

In addition to these effects at equilibrium, both matrix stiffness and residual stress can have an effect on the kinetics, in particular through the kinetics of water diffusion. Indeed, a possible description of the dependency of diffusion coefficient (D_P) with hydrostatic stress (σ_h) and Young's modulus (E) can be given by:

$$D_P = \frac{D_0}{2} exp\left(C_1 \frac{1}{k_B T} \frac{\sigma_h}{E}\right) \qquad (16)$$

Here D_0 is the diffusion coefficient in the absence of stress, C_1 a material-related constant, k_B the Boltzmann constant and T the absolute temperature. Although this relation was established for Bcc metals [35], the fact that the diffusion coefficient varies in opposite ways with increasing hydrostatic stress and increasing matrix stiffness should be preserved in a tetragonal ceramic. As can be seen in Figure 6, here the residual stress increases with matrix stiffness. However, using equations 8 and 14(a) and postulating that the applied stress (σ_h) is equal to the stress in the tetragonal zirconia phase (σ_t), one can calculate that:

$$\frac{\sigma_h}{E} = -\frac{V_a}{1-V_a} \times \frac{3K_a(\alpha_t-\alpha_a)\Delta T V_a(1+n_a)}{(1-V_a)(1+n_a)+V_a(1+n_a\frac{K_a}{K_t})} \times \frac{1}{210.4+133.3V_a+56.3V_a^2} \qquad (17)$$

A very good numerical approximation of the variation of this ratio with *V*a is (with the same unit for σ_h and E):

$$\frac{\sigma_h}{E} = (1.81V_a^3 - 6.35V_a^2 + 8.39V_a) \times 10^{-3} \qquad (18)$$

As a result, with the values given earlier in this section $\frac{\sigma_h}{E}$ increases with the alumina fraction. Thus the observed evolutions of the ageing behaviour with residual stress and matrix stiffness, which imply a decrease of the diffusion coefficient, are compatible with a negative value of C_1, that we have unfortunately no mean to evaluate without ab-initio calculations.

4.3. Effect of zirconia inclusion size

In ZTA25 samples, the different milling procedures lead to a significant difference in the size of zirconia inclusions in the composites. From SEM images, it is found that the order of the average size of zirconia inclusions is: ZTA25-7d < ZTA25-1d < ZTA25-1d8m. The average spectral shifts of zirconia 146 cm^{-1} peak in the corresponding annealed samples respectively are -1.5 cm^{-1}, -1.34 cm^{-1} and -1.26 cm^{-1}. These results indicate that the average tensile stress of the zirconia inclusions decreases as the inclusions size increases. The size of zirconia inclusions has a very important effect on ageing behaviour of ZTA composites. The results on Figure 5 show that ageing often occurs first in the central region of large size zirconia

inclusions where the tensile stress is minimal, and where the local matrix stiffness is also minimal. Larger zirconia particles in the ageing process will lead to more transformation from tetragonal zirconia into monoclinic phase since the zones with low tensile stresses and low matrix stiffness are larger, in coherence with the overall ageing behaviour reported in Figure 8.

5. Conclusion

Several zirconia-toughened alumina ceramics were fabricated, with different microstructures, allowing variation of the local environment of tetragonal zirconia grains (alumina content, size of zirconia agglomerates, residual stresses). The following conclusions can be drawn:

1. The zirconia particles in ZTA composites are mainly subjected to tensile stress, and the stress increases with increasing alumina content with a near- linear relation. The polishing process, triggering a small amount of t-m phase transformation, can lower the average internal tensile stress but increase its distribution width, making more probable the presence of highly stressed zones.
2. The maximum t-m transformation extension after ageing of these ZTA composites has a strong relationship with the distribution of the alumina content, through a balance between local residual tensile stress (destabilizing the t phase) and local matrix stiffness (stiffer matrix stabilizes the t phase): it decreases with increasing alumina content, showing that the matrix stiffness effects is dominant over the residual stresses effect.
3. The presence of tensile stresses slows down the ageing kinetics, an opposite result to what is observed in zirconia monoliths. This may be related to both thermodynamic and kinetic considerations. Thermodynamically, in ZTA composites, the highest tensile stresses (in the zirconia phase) are observed in zones with the highest alumina content and highest stiffness. Both theoretical calculations and experiments confirm the dominance of the stiffness over the internal tensile stresses on the stability of the t-phase, resulting in more stable t-phase with increasing alumina fraction, thus a lower driving force for the t-m transformation and slower kinetics. Moreover, the diffusion coefficient of water is also related to internal stress, however this effect could not be quantified here.
4. These results also emphasize the necessity, when processing ZTA composites, to avoid the presence of large-sized zirconia inclusions, as these inclusions are nuclei of hydrothermal ageing.

Acknowledgments

C. Wei’s PhD thesis at INSA-Lyon was supported by a grant from the Chinese Science Council.

References

[1] J. Chevalier, What future for zirconia as a biomaterial?, Biomaterials. 27 (2006) 535–543. doi:10.1016/j.biomaterials.2005.07.034.

[2] J. Chevalier, L. Gremillard, S. Deville, Low-Temperature Degradation of Zirconia and Implications for Biomedical Implants, Annu. Rev. Mater. Res. 37 (2007) 1–32. doi:10.1146/annurev.matsci.37.052506.084250.

[3] H. Schubert, F. Frey, Stability of Y-TZP during hydrothermal treatment: neutron experiments and stability considerations, J. Eur. Ceram. Soc. 25 (2005) 1597–1602. doi:10.1016/j.jeurceramsoc.2004.03.025.

[4] J. Li, L. Zhang, Q. Shen, T. Hashida, Degradation of yttria-stabilized zirconia at 370K under a low applied stress, Mater. Sci. Eng. A. 297 (2001) 26–30.

[5] C. Wei, L. Gremillard, The influence of stresses on ageing kinetics of 3Y- and 4Y-stabilized zirconia, J. Eur. Ceram. Soc. 38 (2018) 753–760. doi:10.1016/j.jeurceramsoc.2017.09.044.

[6] V. Lughi, V. Sergo, Low temperature degradation -aging- of zirconia: A critical review of the relevant aspects in dentistry, Dent. Mater. 26 (2010) 807–820. doi:10.1016/j.dental.2010.04.006.

[7] S. Deville, J. Chevalier, G. Fantozzi, J.F. Bartolomé, J. Requena, J.S. Moya, R. Torrecillas, L.A. Díaz, Low-temperature ageing of zirconia-toughened alumina ceramics and its implication in biomedical implants, J. Eur. Ceram. Soc. 23 (2003) 2975–2982. doi:10.1016/S0955-2219(03)00313-3.

[8] C. Pecharromán, J.F. Bartolomé, J. Requena, J.S. Moya, S. Deville, J. Chevalier, G. Fantozzi, R. Torrecillas, Percolative Mechanism of Aging in Zirconia- Containing Ceramics for Medical Applications, Adv. Mater. 15 (2003) 507–511.

[9] F.F. Lange, Transformation toughening. 1 Size effects associated with the thermodynamics of constrained transformations, J. Mater. Sci. 17 (1982) 225–234.

[10] G. Pezzotti, A.A. Porporati, Raman spectroscopic analysis of phase-transformation and stress patterns in zirconia hip joints, J. Biomed. Opt. 9 (2004) 372. doi:10.1117/1.1647547.

[11] V. Sergo, D.R. Clarke, W. Pompe, Deformation Bands in Ceria-Stabilized Tetragonal Zirconia/Alumina: I, Measurements of Internal Stresses, J. Am. Ceram. Soc. 78 (1995) 633–40.

[12] G. De Portu, L. Micele, Y. Sekiguchi, G. Pezzotti, Measurement of residual stress distributions in Al 2 O 3 / 3Y-TZP multilayered composites by fluorescence and Raman microprobe piezo-spectroscopy, Acta Mater. 53 (2005) 1511–1520. doi:10.1016/j.actamat.2004.12.003.

[13] J. Chevalier, C. Olagnon, G. Fantozzi, Study of the residual stress field around Vickers indentations in a 3Y-TZP, J. Mater. Sci. 31 (1996) 2711–2717.

[14] H. Toraya, M. Yoshimura, S. Somiya, Calibration curves for the quantitative analysis of the monoclinic-tetragonal ZrO2 system by X-ray diffraction, J. Am. Ceram. Soc. 67 (1984) C119–C121.

[15] R.C. Garvie, P.S. Nicholson, Phases analysis in zirconia systems, J. Am. Ceram. Soc. 55 (1972) 303–305.

[16] J.A. Muñoz-Tabares, M. Anglada, Hydrothermal degradation of ground 3Y-TZP, J. Eur. Ceram. Soc. 32 (2012) 325–333. doi:10.1016/j.jeurceramsoc.2011.08.029.

[17] M. Inokoshi, K. Vanmeensel, F. Zhang, J. De Munck, G. Eliades, S. Minakuchi, I. Naert, B. Van Meerbeek, J. Vleugels, Aging resistance of surface-treated dental zirconia, Dent. Mater. 31 (2015) 182–194. doi:10.1016/j.dental.2014.11.018.

[18] J.A. Muñoz Tabares, M.J. Anglada, Quantitative analysis of monoclinic phase in 3Y-TZP by raman spectroscopy, J. Am. Ceram. Soc. 93 (2010) 1790–1795.

doi:10.1111/j.1551-2916.2010.03635.x.
[19] V. Sergo, D.M. Lipkin, G. De Portu, D.R. Clarke, Edge Stresses in Alumina/Zirconia Laminates, J. Am. Ceram. Soc. 80 (1997) 1633–1638. doi:10.1111/j.1151-2916.1997.tb03031.x.
[20] Q. Ma, D.R. Clarke, Stress Measurement in Single-Crystal and Polycrystalline Ceramics Using Their Optical Fluorescence, J. Am. Ceram. Soc. 76 (1993) 1433–1440. doi:10.1111/j.1151-2916.1993.tb03922.x.
[21] J. Chevalier, B. Cales, J.M. Drouin, Low-Temperature Aging of Y-TZP Ceramics, J. Am. Ceram. Soc. 82 (1999) 2150–2154.
[22] L. Gremillard, J. Chevalier, T. Epicier, S. Deville, G. Fantozzi, Modeling the aging kinetics of zirconia ceramics, J. Eur. Ceram. Soc. 24 (2004) 3483–3489. doi:10.1016/j.jeurceramsoc.2003.11.025.
[23] P.J. Whalen, F. Reidinger, R.F. Antrim, Prevention of Low-Temperature Surface Transformation by Surface Recrystallization in Yttria-Doped Tetragonal Zirconia, J. Am. Ceram. Soc. 72 (1989) 319–321.
[24] C.F. Caravaca, Q. Flamant, M. Anglada, L. Gremillard, J. Chevalier, Impact of sandblasting on the mechanical properties and aging resistance of alumina and zirconia based ceramics, J. Eur. Ceram. Soc. 38 (2018). doi:10.1016/j.jeurceramsoc.2017.10.050.
[25] K. Fan, J. Ruiz-Hervias, J.Y. Pastor, J. Gurauskis, C. Baudín, Residual stress and diffraction line-broadening analysis of Al2O3/Y-TZP ceramic composites by neutron diffraction measurement, Int. J. Refract. Met. Hard Mater. 64 (2017) 122–134. doi:10.1016/j.ijrmhm.2017.01.011.
[26] W. Kreher, Internal Stresses and Relations between Effective Thermoelastic Properties of Stochastic Solids – Some Exact Solutions, ZAMM - J. Appl. Math. Mech. / Zeitschrift Für Angew. Math. Und Mech. 68 (1988) 147–154. doi:10.1002/zamm.19880680311.
[27] W. Kreher, W. Pompe, Internal Stresses in Heterogeneous Solids, Berlin, 1989.
[28] W. Pabst, E. Gregorova, G. Ticha, E. Gregorová, G. Tichá, Elasticity of porous ceramics—A critical study of modulus−porosity relations., J. Eur. Ceram. Soc. 26 (2006) 1085–1097. doi:10.1016/j.jeurceramsoc.2005.01.041.
[29] C.W. Lim, Z.R. Li, L.H. He, Size dependent, non-uniform elastic field inside a nano-scale spherical inclusion due to interface stress, Int. J. Solids Struct. 43 (2006) 5055–5065. doi:10.1016/j.ijsolstr.2005.08.007.
[30] C.Q. Ru, Analytic Solution for Eshelby's Problem of an Inclusion of Arbitrary Shape in a Plane or Half-Plane, J. Appl. Mech. 66 (1999) 315. doi:10.1115/1.2791051.
[31] I. Schmidt, D. Gross, The equilibrium shape of an elastically inhomogeneous inclusion, J. Mech. Phys. Solids. 45 (1997) 1521–1549. doi:10.1016/S0022-5096(97)00011-2.
[32] P. Sharma, S. Ganti, Size-Dependent Eshelby's Tensor for Embedded Nano-Inclusions Incorporating Surface/Interface Energies, J. Appl. Mech. 71 (2004) 663. doi:10.1115/1.1781177.
[33] A. Samodurova, A. Kocjan, M. V. Swain, T. Kosmac, The combined effect of alumina and silica co-doping on the ageing resistance of 3Y-TZP bioceramics, Acta Biomater. 11 (2015) 477–487. doi:10.1016/j.actbio.2014.09.009.
[34] A.G. Gebresilassie, Atomic scale simulations in zirconia : Effect of yttria doping and environment on stability of phases, INSA-Lyon, 2017.
[35] A. V. Nazarov, A.A. Mikheev, Diffusion under a stress in fcc and bcc metals, J. Phys. Condens. Matter. 20 (2008). doi:10.1088/0953-8984/20/48/485203.